

EFFECT OF LARGE-SCALE STRUCTURE ON MULTIPLY IMAGED SOURCES

Rennan Bar-Kana¹
 Department of Physics, MIT, Cambridge, MA 02139 USA

ABSTRACT

We study the effects of large-scale density fluctuations on strong gravitational lensing. Previous studies have focused mostly on weak lensing, since large-scale structure alone cannot produce multiple images. When a galaxy or cluster acts as a primary lens, however, we find that large-scale structure can produce asymmetric shear of the same order as the lens itself. Indeed, this may explain the origin of the large shear found in lens models in conflict with the small ellipticity of the observed galaxy light distributions. We show that large-scale structure changes the lens equation to the form of a generalized quadrupole lens, which affects lens reconstruction. Large-scale structure also changes the angular diameter distance at a given redshift. The precise value depends on the lens and source redshifts and on the large-scale structure power spectrum, but the induced 1σ uncertainty in determinations of the Hubble constant from measurements of time delays is of order 5 – 10%. If observations of lensing can constrain the magnitude of the shear which is due to large-scale structure, it would provide a direct probe of the overall amplitude of mass fluctuations.

Subject headings: gravitational lensing — large-scale structure of universe

1. Introduction

Gravitational lensing is one of the most promising methods of mapping the distribution of matter at cosmological distances. Detailed observations of multiple images of quasars have been used to try and reconstruct the lensing mass distribution (e.g. Falco et al. 1991). It has also long been recognized that measurements of the time delay between images can be used to determine the Hubble constant (Refsdal 1964, 1966). However, practical application to the double quasar 0957+561 has been difficult because of uncertainties in lens modelling as well as conflicting measurements of the time delay (e.g. Vanderriest et al. 1989; Lehár et al. 1992).

Since gravitational lenses and sources typically lie at significant redshifts, light rays are deflected by large-scale structure (LSS) as they traverse the enormous distance from source to observer. These deflections are not large enough to produce multiple images, but they do distort the shapes of sources. Such weak lensing has been investigated both analytically (e.g. Miralda-Escudé 1991; Kaiser 1992) and

¹email: barkana@arcturus.mit.edu

in N-body simulations (Jaroszynski et al. 1991; Blandford et al. 1991). These studies find a shear of order 1%, coherent over a scale of $\approx 1^\circ$, in a flat CDM model. This shear may in principle be detected observationally as a coherent distortion of background galaxies, when averaged over a sufficiently large angular field in order to be separated from the random scatter of intrinsic ellipticities (e.g. Mould et al. 1994; Villumsen 1995).

The shear due to LSS can also affect strong lensing, when it acts in addition to a strong primary lens, a galaxy or cluster near the line of sight to the source. This effect is enhanced compared to weak lensing, because of the small angular separations between multiple images. Also, the higher redshift of quasars compared to faint galaxies increases the cumulative shear from the observer to the source. Seljak (1994) estimated the dependence of the r.m.s. value of this shear on the power spectrum of density fluctuations, and found it to be of order 10% for a source at redshift 3. Seljak also considered the effect of LSS on the time delay, and showed that the lowest order terms cancel out in the total time delay. However, since these canceling terms are separately much larger than the time delay from the primary lens, even higher order terms might still dominate the time delay and threaten the effort to determine the Hubble constant from lensing.

In order to find precisely how LSS affects the observables of a lens system, Surpi et al. (1995) set up the lens equation in the presence of a lens plus LSS. They made an expansion for the position of a light ray in powers of its deflection from the unperturbed straight path, and kept only the lowest order term. This term is equivalent to a constant angular deflection at the lens. They thus concluded that LSS leaves all observables (such as relative image positions) unchanged to lowest order. Indeed, since the actual source position is unobservable, the effect of this lowest order term can be removed from the lens equation by subtracting the constant angle out of the source angle. This approximation of keeping the lowest order term is not a good one, however, since the shear due to LSS arises from *relative* deflections between different light rays, which involve higher order terms in the expansion. We follow a similar approach but include these higher order terms in order to study the observable effects of LSS.

In this paper we analyze the effect of LSS on the lens equation and time delay. Readers primarily interested in the results may wish to concentrate on §4 – §6 and §8. We derive the lens equation in §2 and §3, and find it to have a form similar to the generalized quadrupole lens of Kovner (1987) (§4). We express the perturbed lens equation in terms of integrals along the line of sight of the scalar, Newtonian potential. These integrals are random variables of zero mean, whose variances and covariances can be evaluated in terms of the power spectrum of density perturbations (§5). We find that the effective shear in the lens equation is not simply the integrated shear from the observer to the source, but is reduced by 40% or more, depending on the lens redshift. For realistic power spectra that include modelling of non-linear effects, the effective shear is of order 6% for a source at redshift 3. In addition, the accumulated shear from the observer to the lens can significantly affect the observables as well as the appearance of the lens itself, if the lens is at a relatively high redshift. In §3 we also discuss how our results determine the effect of LSS on angular diameter distances.

The most important effect of shear is in producing four-image systems. Many confirmed lens systems are quads, since they are easy to identify and tend to be highly magnified (Kochanek 1991b,1995; Wallington & Narayan 1993). These systems are inconsistent with an axi-symmetric lens, for which all

the images would have to be colinear. Lens models of quads typically find a shear of order 7 – 11% (e.g. Kochanek 1991a). If due to the lensing galaxy itself, this would imply a projected ellipticity (= 1 minus the ratio of minor to major axis) for the mass of $\approx 35 - 50\%$. By contrast, the typical value observed for ellipticals is $\approx 20\%$ (e.g. Ryden 1992; Schechter 1987). Since the cross-section for producing quads increases with shear, observed quads should be biased towards high shear, whatever its origin (Kassiola & Kovner 1993). In particular this includes a bias toward an alignment between the shear caused by the galaxy and the external shear. High resolution observations of lensing galaxies can determine the degree of agreement or inconsistency between the observed ellipticity and the inferred shear in specific cases. Recent observations of a four-image ‘‘Einstein cross’’ with the Hubble Space Telescope WFPC2 (Ratnatunga et al. 1995) found an ellipticity in the potential of 26%, which implies a mass ellipticity of 60%. The light distribution was found to have an ellipticity of only 32%. One possible explanation is that the dark matter halo is highly flattened compared to the light distribution, but other observations may not support the existence of such large differences in typical galaxies (for a recent review see Sackett 1995). Another possibility is that a LSS shear of order 8% has been added on to the 7% shear of the lens. In fact, the directions of the total shear and that due to the light distributions are different by about 13° , so the disagreement is larger. A recent HST observation of a lensed arc (Eisenhardt et al. 1995) has similarly found an observed ellipticity of about half that implied by the best fit lens model. Note, however that other possible sources of external shear, namely additional galaxies or clusters near the line of sight to the source, must be properly accounted for before the contribution of LSS can be determined.

In §4 we also consider the effect of LSS on relative time delays of images. The related phenomenon of amplification of sources due to large-scale structure has been studied by Babul & Lee (1991), but not in the presence of a primary lens. We show that the effect on time delays is enhanced through a combination of two separate effects. LSS thus limits our ability to derive accurate values of the Hubble constant from lensing. The induced uncertainty depends on the lens and source redshifts and on the large-scale structure power spectrum, but in §5 we find it to be of order 5 – 10% at 1σ . This uncertainty may have either sign since LSS may effectively produce a negative mass density (negative is measured w.r.t. the mean density of the universe, not w.r.t. zero).

In §6 we choose a simple lens distribution, a singular isothermal sphere, and illustrate the effect of LSS on relative image positions and time delays, as well as the caustics and critical curves of the lens system. In §7 we apply our formalism to the transition from strong to weak lensing and demonstrate its agreement with previous studies of weak lensing (a detailed derivation is given in Appendix B). Finally, in §8 we give our conclusions and comment on possible applications of our results.

We assume a flat universe throughout, in the absence of an accurate fitting formula for the time dependent, non-linear power spectrum in a curved background. Our formalism is, however, easily generalized to a closed or open universe, as we show in Appendix A.

2. Formalism

We work in the framework of a flat Robertson-Walker metric with small-amplitude scalar metric fluctuations. In the longitudinal gauge (Bardeen 1980) we can write the line element as

$$ds^2 = a^2(\tau)[-(1 + 2\phi)d\tau^2 + (1 - 2\phi)d\vec{x} \cdot d\vec{x}] , \quad (1)$$

where we set $c = 1$. Here τ is the conformal time, $a(\tau)$ the expansion factor, and we are using comoving coordinates \vec{x} . Redshift in a flat, matter-dominated ($\Omega_m = 1$) universe is given by $1/(1 + z) = a(\tau) = (H_0\tau/2)^2$, with $H_0 = 100h \text{ km sec}^{-1} \text{ Mpc}^{-1}$ the present Hubble constant. Also ϕ is the scalar, Newtonian potential obeying the cosmological Poisson equation

$$\nabla^2\phi = 4\pi G a^2 \bar{\rho} \delta , \quad (2)$$

where $\bar{\rho}$ is the mean density of the universe and $\delta = (\rho - \bar{\rho})/\bar{\rho}$ is the local density perturbation. We describe statistical properties of ϕ in terms of its Fourier transform $\phi(\vec{k}, \tau)$, where $\phi(\vec{x}, \tau) = \int d^3k \phi(\vec{k}, \tau) e^{i\vec{k} \cdot \vec{x}}$. Its ensemble mean and variance are $\langle \phi(\vec{k}, \tau) \rangle = 0$ and $\langle \phi(\vec{k}, \tau) \phi^*(\vec{k}', \tau) \rangle = P_\phi(k, \tau) \delta^3(\vec{k} - \vec{k}')$, where $P_\phi(k, \tau)$ is the power spectrum of the potential at time τ , simply related to the density power spectrum by $P_\phi(k, \tau) = (4\pi G a^2(\tau) \bar{\rho}(\tau))^2 k^{-4} P_\rho(k, \tau)$.

We place the observer at the origin of coordinates and the primary lens² on the z -axis. We use r to denote values of the z -coordinate, with z_L and z_S reserved for lens and source redshift, respectively. Note that the z -axis is only a coordinate axis used for reference and not the actual path of any light ray. We let \vec{n} denote a unit vector in the photon's direction of motion and \vec{x} denote its position. To first order in ϕ , in the metric (1) they obey

$$\frac{d\vec{n}}{d\tau} = -2 \left[\vec{\nabla}\phi - \vec{n}(\vec{n} \cdot \vec{\nabla}\phi) \right] , \quad \frac{d\vec{x}}{d\tau} = \vec{n}(1 + 2\phi) . \quad (3)$$

In this and similar expressions in this section, ϕ is to be evaluated on the actual photon path, not on the z -axis.

We now assume that the angle between \vec{n} and the z -axis is small (e.g. Seljak 1994), and consider the components perpendicular to the z -axis of \vec{n} and \vec{x} . They obey

$$\frac{d\vec{n}_\perp}{d\tau} = -2\vec{\nabla}_\perp\phi , \quad \frac{d\vec{x}_\perp}{d\tau} = \vec{n}_\perp , \quad (4)$$

where $\vec{\nabla}_\perp\phi$ denotes the derivative of the potential transverse to the z -axis. In the approximation of small angles, these equations are the same as the Newtonian equations of motion for a particle moving in a gravitational field, except for the factor of 2 from General Relativity. The absolute mean of ϕ is not observable, since the perturbations in the metric are defined about the large-scale mean. Indeed, we may choose our space and time units so that the large-scale value of ϕ is zero at the Local Group. Then ϕ is a random variable with r.m.s. value of order 10^{-4} for the observed LSS power spectrum.

²“The lens” refers to some reference point in the lens plane, such as the center if the lens is axi-symmetric.

Equation (3) implies that the photon path obeys $r(\tau) = \tau_0 - \tau$ with $O(\phi)$ corrections, where τ_0 is the present value of τ . The relation of comoving distance to redshift is, e.g. in an Einstein-de Sitter universe, $r(z) = 2H_0^{-1}[1 - (1+z)^{-1/2}]$. Thus comoving distances are simply related to the measured redshifts (to $O(\phi)$), and so we use comoving distances rather than angular diameter distances (r_L and r_S refer below to the lens and source, respectively). In a homogeneous universe with no LSS, angular diameter distances are given by $D = r/(1+z)$. In general, if an object at comoving distance r has a proper diameter R and is observed to subtend an angle θ , then the angular diameter distance is defined to be $D = R/\theta$. This differs from D in the homogeneous case by terms larger than $O(\phi)$. As explained in §1, this is precisely the effect which we calculate below, and so we discuss angular diameter distances further in §3.

We can trace the photon trajectory backwards in time using equations (4), with the final conditions $\vec{x}_\perp = 0$ and $\vec{n}_\perp = \vec{n}_\perp^0$ at the observer $r = 0$. Between the observer and the lens, we find that

$$\begin{aligned}\vec{n}_\perp(\tau) &= \vec{n}_\perp^0 + 2 \int_\tau^{\tau_0} \vec{\nabla}_\perp \phi(\tau') d\tau' , \\ \vec{x}_\perp(\tau) &= -(\tau_0 - \tau)\vec{n}_\perp^0 - 2 \int_\tau^{\tau_0} (\tau' - \tau)\vec{\nabla}_\perp \phi(\tau') d\tau' .\end{aligned}\tag{5}$$

When the photon is at the lens, its direction of motion is $\vec{n}_\perp(\tau_L)$. It is then deflected so that at the source side of the lens its direction of motion is $\vec{p}_\perp = \vec{n}_\perp(\tau_L) + \vec{\gamma}$. The deflection angle $\vec{\gamma}$ is evaluated at $\vec{x}_\perp^L \equiv \vec{x}_\perp(\tau_L)$, and is determined by the mass distribution of the primary lens. Equations (4) then imply that, between the lens and the source,

$$\begin{aligned}\vec{n}_\perp(\tau) &= \vec{p}_\perp + 2 \int_\tau^{\tau_L} \vec{\nabla}_\perp \phi(\tau') d\tau' , \\ \vec{x}_\perp(\tau) &= \vec{x}_\perp(\tau_L) - (\tau_L - \tau)\vec{p}_\perp - 2 \int_\tau^{\tau_L} (\tau' - \tau)\vec{\nabla}_\perp \phi(\tau') d\tau' .\end{aligned}\tag{6}$$

For a given source position \vec{x}_\perp^S , the lens equation is then $\vec{x}_\perp(\tau_S) = \vec{x}_\perp^S$.

The total proper time delay, relative to the $\phi = 0$ path along the z -axis, is given by (e.g. Schneider et al. 1992)

$$\Delta t = \int_{\tau_S}^{\tau_0} \left[\frac{1}{2} \left(\frac{d\vec{x}_\perp}{d\tau} \right)^2 - 2\phi \right] d\tau - (1 + z_L)\psi(\vec{x}_\perp^L) .\tag{7}$$

The first term is the geometrical time delay, the second is the potential time delay due to LSS, and the last is the potential time delay due to the lens, given by

$$\psi(\vec{x}_\perp) = 4G \int d^2\xi' \Sigma(\vec{\xi}') \log \left| \frac{\vec{\xi} - \vec{\xi}'}{(1 + z_L)^{-1} r_L} \right| ,\tag{8}$$

where $\Sigma(\vec{\xi})$ is the projected mass density of the lens, and $\vec{\xi} = (1 + z_L)^{-1} \vec{x}_\perp$ measures *proper* distance in the lens plane. We let $r_{LS} = r_S - r_L$, and then the scaled deflection angle is given by

$$\vec{\alpha} = \frac{r_{LS}}{r_S} \vec{\gamma} = \frac{r_{LS}}{r_S} \frac{\partial \psi}{\partial \vec{\xi}} .\tag{9}$$

3. Lensing in the presence of LSS

Equations (5) and (6) cannot in general be solved analytically, since they involve integrals over the potential ϕ evaluated on the (unknown) photon path. We therefore expand ϕ about its value on the z -axis (as in Surpi et al. 1995):

$$\phi(r\hat{z} + \vec{x}_\perp) \approx \phi + \vec{x}_\perp \cdot \vec{\nabla}_\perp \phi + \frac{1}{2}(\vec{x}_\perp \cdot \vec{\nabla}_\perp)^2 \phi, \quad (10)$$

where the right-hand side (RHS) is evaluated on the z -axis. The second term on the RHS leads to an unobservable constant deflection, and the third to a relative deflection between light rays. Unlike Surpi et al., we include the third term. To lowest order, in the resulting expansion for $\vec{\nabla}_\perp \phi$ we substitute for \vec{x}_\perp the expressions given in equations (5) and (6) with ϕ evaluated on the z -axis. Hereafter, all expressions involving ϕ are evaluated on the z -axis.

The expansion (10) should be valid as long as the LSS power on scales smaller than the deflection \vec{x}_\perp is negligible. We find below, however, that the shear is produced by modes over a broad range of wavelengths. Moreover, the higher order terms in the expansion formally diverge at small wavelengths in an r.m.s. sense, e.g. for a scale-invariant spectrum, at fixed \vec{x}_\perp . In reality, \vec{x}_\perp depends on the initial direction and on ϕ . This worry is resolved by using a different expansion, equivalent to summing this entire series (see §7). This alternate expansion is convergent, and shows that the contribution of small wavelength modes is cut off. For strong lensing we find that the terms in equation (10) suffice for an accurate analysis. Note that we have not assumed at any point that $\delta < 1$ for the density. Our expansions remain valid even when we include non-linear modes for which $\delta \gg 1$.

We are not interested in any deflection which is common to all light rays, since such a constant angle only affects the unobservable absolute position of the source. We can subtract out such terms to all orders simply by measuring displacements relative to some light ray instead of the z -axis. We define this fiducial ray as the light ray (null geodesic) passing through the observer and through the lens, and extended out to r_S (see figure 1). This ray is deflected by LSS throughout its path, but is not deflected by the primary lens. The quantities \vec{x}_\perp and \vec{n}_\perp measured relative to the corresponding quantities for this fiducial ray we denote by \vec{d}_\perp and \vec{l}_\perp , respectively. Then $\vec{\theta} = -\vec{l}_\perp^0$ is the observed angle of a light ray relative to the observed lens position. Note that $\vec{d}_\perp^L = \vec{x}_\perp^L \equiv r_L \vec{X}$.

We define dimensionless 2×2 symmetric tensors,

$$\begin{aligned} F_{ij}(\tau_1, \tau_2) &= -\frac{2}{\tau_1 - \tau_2} \int_{\tau_2}^{\tau_1} (\tau - \tau_2)(\tau_1 - \tau) \partial_i \partial_j \phi(\tau) d\tau, \\ G_{ij}(\tau_1, \tau_2) &= -2 \int_{\tau_2}^{\tau_1} (\tau_1 - \tau) \partial_i \partial_j \phi(\tau) d\tau. \end{aligned} \quad (11)$$

The traceless part of F_{ij} is the shear tensor of weak lensing (e.g. Kaiser 1992).

Between the observer and the lens,

$$\begin{aligned} l_\perp^i(\tau) &= -\theta^i - \theta_j G^{ij}(\tau_0, \tau), \\ d_\perp^i(\tau) &= (\tau_0 - \tau) \left[\theta^i + \theta_j F^{ij}(\tau_0, \tau) \right]. \end{aligned} \quad (12)$$

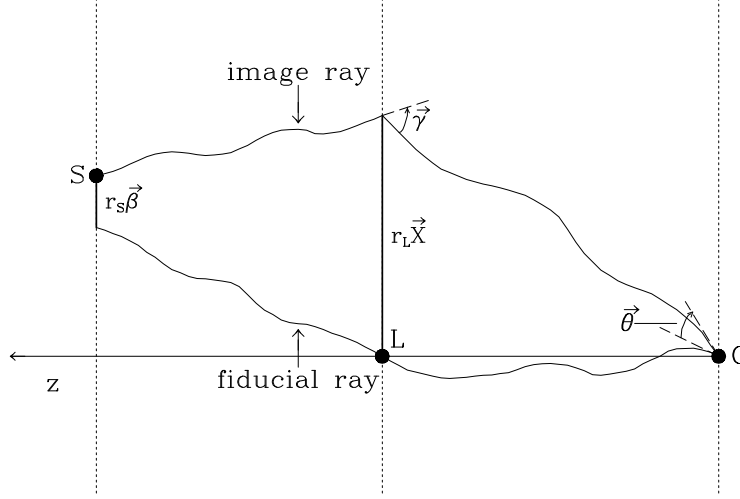


Fig. 1.— Sketch showing the fiducial ray and an image ray, with distances in comoving coordinates.

Equations (12) suggest a simple physical interpretation for the two tensors, in our approximation. For two rays that end up at the origin at τ_0 with a small angular separation $\vec{\theta}$, $(\tau_0 - \tau)F_{ij}\theta^j$ ³ measures the change in their relative separation at τ , compared to having no LSS. $G_{ij}\theta^j$ similarly measures the induced change in their relative directions at time τ .

If we let $\vec{p}_\perp = \vec{l}_\perp(\tau_L) + \vec{\gamma}(\vec{d}_\perp^L)$ then, between the lens and the source,

$$\begin{aligned} l_\perp^i(\tau) &= p_\perp^i + p_\perp^j G_j^i(\tau_L, \tau) - d_\perp^j(\tau_L) [G_j^i(\tau_L, \tau) + G_j^i(\tau, \tau_L)] / (\tau_L - \tau) , \\ d_\perp^i(\tau) &= d_\perp^i(\tau_L) - (\tau_L - \tau) [p_\perp^i + p_\perp^j F_j^i(\tau_L, \tau)] + d_\perp^j(\tau_L) G_j^i(\tau, \tau_L) . \end{aligned} \quad (13)$$

The lens equation is $\vec{d}_\perp(\tau_S) = \vec{d}_\perp^S$.

Defining $\vec{\beta} = \vec{d}_\perp^S / r_S$, and denoting e.g. $F^{ij}(\tau_0, \tau_L)$ by F_{OL}^{ij} , the lens equation becomes

$$\beta^i = \theta^i + \theta_j F_{OS}^{ij} - (\alpha^i + \alpha_j F_{LS}^{ij}) , \quad (14)$$

where $\vec{\alpha}$ is evaluated at

$$d_\perp^i(\tau_L) = r_L(\theta^i + \theta_j F_{OL}^{ij}) . \quad (15)$$

We thus conclude that to our order of approximation, LSS affects the lens equation through three terms, which are easily understood. Two rays separated by an angle θ^i at the observer would, in the absence of lensing or LSS, be separated by a (comoving) distance $r_L\theta^i$ at the lens and $r_S\theta^i$ at the source. The LSS shear changes these distances to $r_L(\theta^i + \theta_j F_{OL}^{ij})$ and $r_S(\theta^i + \theta_j F_{OS}^{ij})$ respectively. The deflection between the two rays by an angle $-\gamma^i$ at the lens leads to an additional separation of $-r_{LS}\gamma^i = -r_S\alpha^i$ at the source, or $-r_S(\alpha^i + \alpha_j F_{LS}^{ij})$ when we include the effect of LSS shear. There are no cross-terms between these three effects in our approximation, where only terms linear in $\vec{\theta}$ and $\vec{\alpha}$ appear in \vec{d}_\perp .

³Repeated indices are summed over the x and y directions. There is no distinction between upper and lower indices.

The magnification matrix is

$$\frac{\partial\beta^i}{\partial\theta_j} = \delta^{ij} - (-F_{OS}^{ij} + \Psi^{ij} + \Psi_k^i F_{OL}^{kj} + \Psi_k^j F_{LS}^{ki}), \quad (16)$$

where $\Psi^{ij} = \partial_{\xi_i} \partial_{\xi_j} \psi / (4\pi G \Sigma_{cr})$ is the shear matrix of the primary lens, in units of $\Sigma_{cr} = r_S(1 + z_L) / (4\pi G r_L r_{LS})$, and Ψ^{ij} in equation (16) is evaluated at \vec{d}_\perp^L . With the usual sign conventions in lensing, the constant LSS shear is $-F_{OS}^{ij}$. This term would still be present even in the absence of the lens (see §7 below). Note that $\partial\beta^i/\partial\theta_j$ is in general *not* symmetric, which it would be in the absence of LSS. In other words, LSS can rotate images.

As noted in §1, we have also calculated the effect of LSS on angular diameter distances. Indeed, an object which subtends an angle $\vec{\theta}$ at the observer measures a comoving distance \vec{d}_\perp^L on the lens plane, given by equation (15). The same object measures a proper distance $\vec{R} = \vec{d}_\perp^L / (1 + z_L)$, which follows (to $O(\phi)$) from the line element (1) taken at constant τ . Then $R^i = D_{OL}^{ij} \theta_j$, where the angular diameter “distance” $D_{OL}^{ij} = (\delta^{ij} + F_{OL}^{ij}) r_L / (1 + z_L)$ is a tensor when LSS is present. Thus R at a given θ depends on orientation, and also \vec{R} may have a different direction than $\vec{\theta}$, so when giving “distances” to lenses it is preferable to use the comoving distance r_L which is well defined (up to corrections of $O(\phi)$, i.e. 0.01%) in terms of z_L . As we show in §5, the components of F_{OL} are of order a few percent, much larger than $O(\phi)$ corrections. Some other authors (e.g. Ehlers & Schneider 1986, Watanabe et al. 1992, Sasaki 1993) have also considered the effect of LSS on angular diameter distances, but they used an oversimplified model in which some fraction of the mass density in the universe is distributed in clumps. Theory and observation of LSS indicate that a description in terms of a random field with positive and negative fluctuations over a range of scales is more realistic (see also the related discussion in Seljak 1994).

4. The Lens Equation and Time Delay

The lens equation (14) is similar in form to the generalized quadrupole lens of Kovner (1987). Kovner considered multiple lensing in which there is one primary lens and additional lenses with linear deflection laws. In that case Kovner showed how to write the lens equation in the form of a thin-lens equation, which simplifies the analysis of properties of the lens mapping, such as image multiplicities and the time delay between images. LSS is different in that the deflection is accumulated continuously, but the final result can be similarly simplified. Letting

$$X^i = \theta^i + \theta_j F_{OL}^{ij}, \quad (17)$$

$$Y^i = \beta^i - \beta_j F_{LS}^{ij}, \quad (18)$$

the lens equation becomes

$$Y^i = X^i - [X_j F_{\text{eff}}^{ij} + \alpha^i(\vec{X})], \quad (19)$$

$$F_{\text{eff}}^{ij} = -F_{OS}^{ij} + F_{LS}^{ij} + F_{OL}^{ij}, \quad (20)$$

where we write $\vec{\alpha}$ as a function of \vec{X} rather than $r_L \vec{X}$. We find that $\delta^{ij} - F_{\text{eff}}^{ij}$ plays the same role as the “telescope matrix” of Kovner, which in his case is in general symmetric. We find a symmetric F_{eff} only

because we are working to first order in the LSS shear. The effective shear F_{eff}^{ij} is in general significantly weaker than F_{OS}^{ij} , as we show in §5. Still, this shear should be of order 6% r.m.s., compared e.g. with a galaxy of ellipticity 20%, which produces a shear of $\approx 4\%$.

We thus have a simple description of the lens mapping: The source plane is slightly distorted to become the \vec{Y} plane, as given by equation (18), so e.g. a circular source appears elliptical in the \vec{Y} plane. Equation (19) then gives the lens mapping from the \vec{Y} plane to the \vec{X} plane. Finally, the (observed) image plane is also a slightly distorted picture of the \vec{X} plane, as in equation (17). Only the $\vec{Y} \mapsto \vec{X}$ map is non-linear, and it determines the geometry of the lens mapping. Thus e.g. the probability of producing quads depends on the sum of F_{eff} and any intrinsic asymmetric shear from the ellipticity of the lens galaxy. The shear F_{eff} should tend to make the observed galaxy light distribution inconsistent with the observed lensing. If the lens is at high redshift, however, then the distortion in equation (17) is also important, since $\vec{\theta}$ is observed and not \vec{X} . In this case, the lens itself is distorted by LSS, if it is observed. Because this induced ellipticity is likely to be wrongly interpreted as intrinsic to the galaxy, it tends to confuse observers as to the actual direction of the galaxy’s internal shear, but the effect is important only if the intrinsic ellipticity itself is not too large. Since the source plane is not directly observable, the distortion in equation (18) does not affect lens reconstruction, but it is important for absolute magnifications (given by equation (16)), and for measuring shape distortions (§7).

We can calculate the time delay explicitly using equation (7). However, it is easier to use Fermat’s principle, which implies that (for a given $\phi(\vec{x}, \tau)$) the lens equation must be equivalent to $\partial\Delta t/\partial\vec{\theta} = 0$ at fixed $\vec{\beta}$ (e.g. Schneider et al. 1992). Thus the time delay is the same as that corresponding to the thin-lens equation (19) which, up to \vec{X} -independent terms, equals (Kovner 1987)

$$\Delta t = \frac{1}{2} \frac{r_L r_S}{r_{LS}} \left[(\vec{X} - \vec{Y})^2 - F_{\text{eff}}^{ij} X_i X_j \right] - (1 + z_L) \psi(r_L \vec{X}) . \quad (21)$$

We might have expected linear terms of the form $\theta^i C_i$ to make large contributions to Δt , where C_i is independent of $\vec{\theta}$ and $\vec{\beta}$, e.g. $C_i = r_{LS} \int_{\tau_S}^{\tau_L} \partial_i \phi(\tau) d\tau$ or $C^i = F_{LS}^{ij} \int_{\tau_S}^{\tau_L} (\tau_L - \tau) \partial_j \phi(\tau) d\tau$. Such terms do appear in the geometric and potential time delays, but Fermat’s principle shows that they must drop out in the total time delay. These cancellations can also be demonstrated explicitly with equation (7).

In addition to shear effects, the lens geometry is also affected by the trace parts of F_{eff} and F_{OL} . These traces cannot be determined through lens reconstruction, since they only affect the unobservable overall scales of the lens size and distance. However, they do affect the determination of the Hubble constant from lensing. To show the various effects, we first set $F_{OL}^{ij} = 0$, and consider just equation (19) and the effect of the trace part of F_{eff} . We also allow for a focusing term κ_{cl} due to a cluster surrounding the lens galaxy. Equation 5 of Narayan (1991) applies here:

$$\Delta t \propto \sigma^2 r_L , \quad (22)$$

where σ represents some characteristic velocity of the lens system. The proportionality constant in this equation depends on a number of parameters which can in principle be determined for each pair of images from lens modelling. One of these parameters involves σ and κ_{cl} , in the combination

$$\zeta = \frac{r_S}{\sigma^2 r_{LS}} \left[1 - \left(\frac{1}{2} \text{Tr } F_{\text{eff}} + \kappa_{\text{cl}} \right) \right] \quad (23)$$

(as follows from equation 6 of Narayan (1991)). Thus if Δt is measured (and σ is not) then from the product $\zeta \Delta t$, we can try to deduce H_0 given z_L , z_S , and an assumed deceleration parameter q_0 . The real H_0 is different from the H_0 deduced assuming $\kappa_{\text{cl}} = \text{Tr } F_{\text{eff}} = 0$ by a factor of $[1 - (\frac{1}{2} \text{Tr } F_{\text{eff}} + \kappa_{\text{cl}})]$. If both Δt and σ can be measured independently, then as noted in Narayan (1991) we can (if $F_{OL}^{ij} = 0$) circumvent the unknowns in equation (23) and use equation (22) to obtain r_L directly, and thus H_0 for an assumed q_0 .

We now add in also the effect of the trace part of F_{OL} in equation (17), which is an unobservable magnification of the lens plane produced by foreground structure. Since the time delay is proportional to the square of the angular scale (e.g. Schneider et al. 1992), equation (22) is replaced by

$$\Delta t \propto \sigma^2 r_L \left(1 + \frac{1}{2} \text{Tr } F_{OL} \right)^2 . \quad (24)$$

Reasoning as above, we see that if only Δt is measured then (from equations (23) and (24)) the real global H_0 is different from the deduced H_0 (for an assumed q_0) by a factor of $[1 + \frac{1}{2} \text{Tr}(2F_{OL} - F_{\text{eff}}) - \kappa_{\text{cl}}]$, to linear order. LSS thus produces a 1σ uncertainty in determinations of H_0 of

$$\sigma_{H_0,1} = \text{r.m.s. of } \frac{1}{2} \text{Tr } (2F_{OL} - F_{\text{eff}}) . \quad (25)$$

Contrary to Falco et al. (1985), we cannot derive an upper bound on H_0 from the Δt measurement since while $\kappa_{\text{cl}} \geq 0$, the LSS term may be negative or positive. Even with measurements of both Δt and σ^2 , we cannot measure H_0 exactly, since when we use equation (24) we are subject (for a given q_0) to a 1σ uncertainty of

$$\sigma_{H_0,2} = \text{r.m.s. of } \text{Tr } F_{OL} . \quad (26)$$

Thus, LSS creates uncertainties in determinations of the Hubble constant from lensing which apply even to perfect lens models determined by an arbitrarily large number of observables. If a precise measurement of H_0 is sought from lens time delays, then at least for some redshifts and LSS power spectra these uncertainties may not be very small, as we show in §5.

5. LSS effects in realistic models

We have shown above that the effects of LSS on lensing enter through the symmetric tensors F_{OL} , F_{LS} and F_{OS} . For a given lens and source, these tensors will affect the lens mapping as we showed in §4, possibly with observable effects which we illustrate in §6. In this section we estimate the typical magnitude of these tensors that is expected based on theory and observation of LSS, and its dependence on the redshifts of the lens and source.

The tensor components are random variables of zero mean, with variances and covariances given in terms of the power spectrum of ϕ . For example, if $\tau_1 \geq \tau_2 \geq \tau_3$, then following the method of Kaiser (1992) we find that

$$\langle F_{ij}(\tau_1, \tau_2) F_{kl}(\tau_1, \tau_3) \rangle = 2\pi^2 Q_{ijkl} \int_0^\infty k^5 dk \int_{\tau_2}^{\tau_1} \frac{(\tau - \tau_2)(\tau_1 - \tau)}{\tau_1 - \tau_2} \frac{(\tau - \tau_3)(\tau_1 - \tau)}{\tau_1 - \tau_3} P_\phi(k, \tau) d\tau , \quad (27)$$

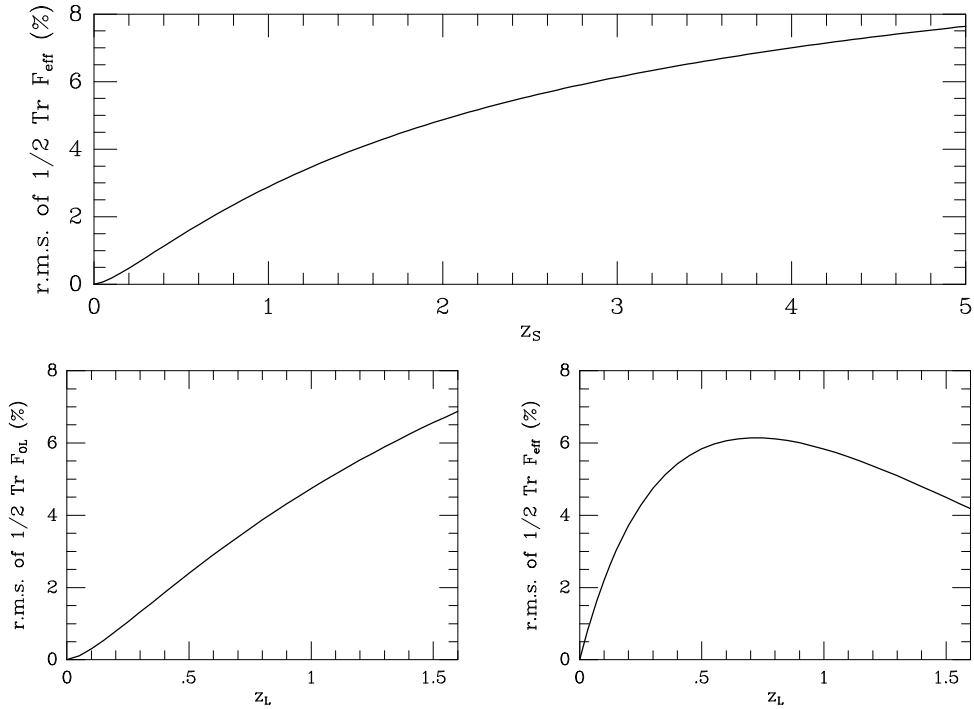


Fig. 2.— The top plot shows the r.m.s. value of $\frac{1}{2} \text{Tr } F_{\text{eff}}$, as a function of z_S , with z_L set so that $r_L = \frac{1}{2}r_S$. The bottom right plot shows the same quantity, but as a function of z_L , for fixed $z_S = 3$. The bottom left plot shows the r.m.s. value of $\frac{1}{2} \text{Tr } F_{OL}$ as a function of z_L . All curves use the non-linear power spectrum, with $\Omega_m = 1$, $h = 0.25$, and $\sigma_8 = 0.8$.

$$\text{where } Q_{ijkl} = \begin{cases} 3 & \text{if } ijkl \text{ are all equal.} \\ 1 & \text{if of } ijkl \text{ two} = x \text{ and two} = y. \\ 0 & \text{otherwise.} \end{cases}$$

This assumes that the dominant contribution comes from modes with wavelengths that are much smaller than the distance $\tau_1 - \tau_2$. This is satisfied for standard forms of the power spectrum and relevant distances.

We follow the approach of Seljak (1995) for calculating r.m.s. shear. For the linear power spectrum we take a scale-invariant spectrum with a CDM type transfer function (Bardeen et al. 1986), which is normalized by σ_8 , the mass fluctuation averaged over a sphere of radius $8h^{-1}$ Mpc, and whose peak is determined by $\Omega_{m0}h$. Galaxy and cluster surveys are consistent with $\sigma_8 \approx 0.8$ and $\Omega_{m0}h \approx 0.25$ (e.g. Peacock & Dodds (1994)). We then find the non-linear power spectrum using the mapping proposed by Hamilton et al. (1991) and extended by Peacock & Dodds (1994), in the improved form of Jain et al. (1995), which they show agrees with N-body simulations at the relevant scales, for an $\Omega_m = 1$ universe. We find that the dominant contribution in equation (27) comes from wavenumbers $k \approx 3 \text{ h Mpc}^{-1}$, with a broad range of two decades on each side contributing significantly. We therefore require a power spectrum that is accurate well into the non-linear regime.

The shear due to F_{OS} is defined as $\Gamma = \sqrt{(\Gamma_1)^2 + (\Gamma_2)^2}$, where $\Gamma_1 = \frac{1}{2}(F_{OS}^{11} - F_{OS}^{22})$ and $\Gamma_2 = F_{OS}^{12}$. Equation (27) shows that Γ has the same r.m.s. value as $\frac{1}{2} \text{Tr } F_{OS}$, which is the convergence or surface mass density κ due to F_{OS} . The same is true for F_{eff} . Because each of the tensors F_{OL} and F_{LS} is

correlated (and so tends to be aligned) with F_{OS} , F_{eff} tends to have smaller components than F_{OS} . For a given z_S , the r.m.s. shear of F_{eff} is maximized at $\approx 60\%$ of that of F_{OS} , approximately at z_L for which $r_L = \frac{1}{2}r_S$. In the top plot of figure 2 we show the r.m.s. value of $\frac{1}{2} \text{Tr } F_{\text{eff}}$ as a function of z_S , at this maximizing z_L . In the bottom right plot we show the same quantity, but as a function of z_L , for a fixed source at redshift 3. This quantity can be estimated for other redshifts through its scaling $\propto r_L r_{LS} / \sqrt{r_S}$, which is accurate to better than 10%. The bottom left plot shows the r.m.s. value of $\frac{1}{2} \text{Tr } F_{OL}$ as a function of z_L . This quantity scales approximately as $\propto r_L^{3/2}$, and also equals $\frac{1}{2}\sigma_{H_0,2}$ as shown in §4. All curves use the non-linear power spectrum, which gives r.m.s. shear larger than the linear spectrum by a factor of ≈ 2.5 . Equation (27) gives a statistical tendency for perpendicular alignment between F_{OL} and F_{eff} , which increases $\sigma_{H_0,1}$ relative to $\frac{1}{2} \text{Tr } F_{\text{eff}}$. At $z_S = 3$ and $r_L = \frac{1}{2}r_S$, $\sigma_{H_0,1} = 11.7\%$, and it scales approximately as $\propto r_L \sqrt{r_S - r_L/3}$. Since the effect of LSS accumulates over distance, we find that the induced shears and time delay uncertainties are all smaller at lower redshifts. For the 0957+561 redshifts ($z_L = .36, z_S = 1.41$), the r.m.s. $\frac{1}{2} \text{Tr } F_{\text{eff}}$ is 3.7%, $\sigma_{H_0,1} = 5.9\%$, and $\sigma_{H_0,2} = 3.3\%$. In addition, note that the effects of LSS on lens reconstruction disappear as $z_L \rightarrow 0$, even if z_S is large.

The r.m.s. shear increases with σ_8 , in exact proportion for the linear power spectrum, faster for the non-linear spectrum. The r.m.s. shear also grows with h (at fixed σ_8), by $\approx 35\%$ for $h = 0.5$ compared to $h = 0.25$. As an additional example, tilted CDM (e.g. Cen et al. 1992) with $h = 0.5$, $\sigma_8 = .6$, and power spectrum index $n = 0.8$ lowers the shear by $\approx 30\%$ compared to Figure 2. The r.m.s. shear can also be calculated for models with $\Omega_{m0} \neq 1$ with modified formulas (see Appendix A).

6. Illustration of the effect of LSS

Kovner (1987) analyzed in some generality the properties of the lens mapping for an axi-symmetric lens perturbed by a weak shear. We simply wish to illustrate the possible observable effects of a shear of the magnitude that we obtained in §5. We choose a particular symmetric lens distribution, a singular isothermal sphere, with deflection law $\vec{\alpha}(r_L \vec{\theta}) = \vec{\theta}/\theta$. We use equations (14) – (16) to find the caustics and critical curves of the lens system. The critical curves are the points in the image plane for which the magnification $\det^{-1}(\partial\beta^i/\partial\theta_j)$ is infinite, and the caustics are the corresponding points in the source plane. The caustics also determine image multiplicities, in that a source located outside all the caustics has a single image, and each time a source moves inside a caustic two images are added (except that for a singular surface density, one image is captured in the core when multiple images are produced). For a given source position, we can thus find all image positions, magnifications, and also time delays with equation (21).

The components F_{OL}^{ij} , etc. are random variables, with covariances obtained as in §5 above. We choose $z_L = 0.78$ and $z_S = 3.0$, and take a particular example:

$$F_{OL} = \begin{pmatrix} -3.87 & 0.50 \\ 0.50 & -2.04 \end{pmatrix} \% , F_{LS} = \begin{pmatrix} -0.70 & 3.68 \\ 3.68 & 2.20 \end{pmatrix} \% , F_{\text{eff}} = \begin{pmatrix} 6.65 & -6.56 \\ -6.56 & -0.31 \end{pmatrix} \% .$$

Figure 3 shows the caustics in the source plane (upper panels) and critical curves in the image plane (lower panels), for the lens alone and for the lens plus LSS. For the latter case, the \vec{Y} (distorted source)

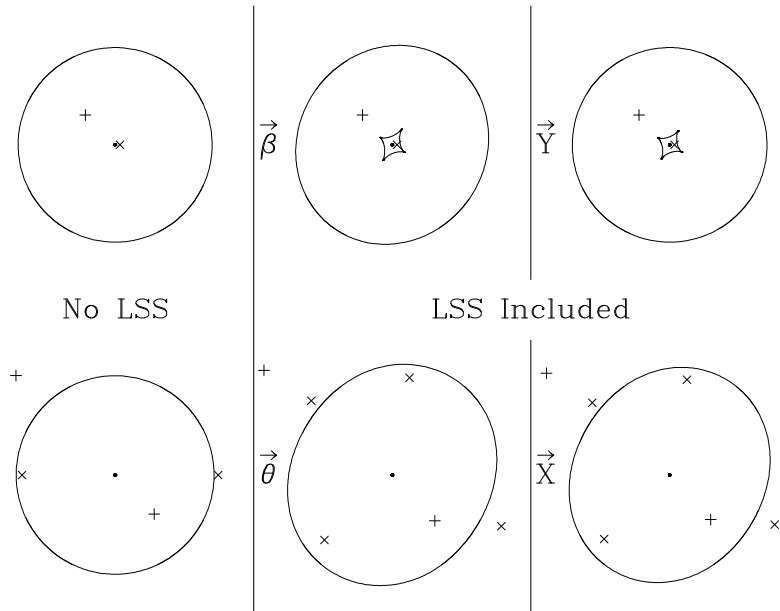


Fig. 3.— Caustics in the source plane (upper panels) and critical curves in the image plane (lower panels) for a singular isothermal sphere, with no LSS, and with LSS. For the latter case, the \vec{Y} (distorted source) plane and \vec{X} (lens) plane are also shown. Also plotted are two source positions (marked + and \times) and the corresponding images for each. A dot shows the $\vec{\theta} = \vec{\beta} = 0$ position.

plane and \vec{X} (lens) plane are also shown. Also plotted are two source positions and the corresponding image positions. Table 1 lists the image positions, magnifications, and relative time delays. LSS changes the image configurations significantly. It displaces images from the line to the lens, in the two-image configuration, and also produces four-image systems when $|\vec{\beta}|$ is small.

7. Weak Lensing and Strong Lensing

The approximation of equation (10) suffices for consideration of strong lensing, where $|\vec{\theta}|$ is very small (\approx a few arcseconds). In weak lensing, however, the shear is observed at larger angles (arcminutes), and the variation of LSS shear with angle is important. Moreover, as noted above, there are potential convergence problems with our expansion of ϕ , even in the strong lensing case. Our formalism allows us to make a more rigorous and powerful expansion, and to study the transition from strong to weak lensing. Note that for shape distortions we must use $\vec{\beta}$ and $\vec{\theta}$ rather than \vec{Y} or \vec{X} , since we are interested in the observed compared to the intrinsic ellipticity of background galaxies.

We replace equation (10) with

$$\phi(r\hat{z} + \vec{x}_\perp) = \sum_{n=0}^{\infty} \frac{1}{n!} (\vec{x}_\perp \cdot \vec{\nabla}_\perp)^n \phi(r\hat{z}), \quad (28)$$

where this expression must be consistent with equations (5) and (6) for \vec{x}_\perp . We now include derivatives to all orders in equation (28), but only keep terms linear in ϕ . This means that in the following expansions

Source at $\vec{\beta} = (-0.30, 0.30)$, $\vec{Y} = (-0.31, 0.30)$				
	Image Plane ($\vec{\theta}$)	Lens Plane (\vec{X})	Magnification	Relative Δt
No LSS	(-1.00, 1.00)	—	3.36	—
	(0.39, -0.39)	—	-1.36	0.84
With LSS	(-1.30, 1.05)	(-1.24, 1.03)	2.82	—
	(0.43, -0.46)	(0.41, -0.45)	-2.05	0.98
Source at $\vec{\beta} = \vec{Y} = (0.05, 0)$				
No LSS	(1.04, 0)	—	21.0	—
	(-0.94, 0)	—	-19.0	0.099
With LSS	(1.10, -0.52)	(1.06, -0.50)	6.18	—
	(-0.82, 0.75)	(-0.78, 0.73)	11.2	0.098
	(0.18, 0.98)	(0.17, 0.96)	-9.22	0.121
	(-0.68, -0.66)	(-0.66, -0.65)	-5.85	0.165

Table 1: Positions of the images shown in figure 3. Also listed are the absolute magnifications (with a sign giving the image parity), and the time delay in units of r_{LS}/r_S relative to the earliest image to arrive at the observer.

in powers of $\vec{\theta}$ and $\vec{\gamma}$, we are finding each coefficient up to relative corrections of the same order as the r.m.s. LSS shear.

Between the observer and the lens, equation (5) requires

$$\vec{x}_\perp(\tau) = -(\tau_0 - \tau)\vec{n}_\perp^0 - 2 \int_\tau^{\tau_0} (\tau' - \tau) e^{\vec{x}_\perp(\tau') \cdot \vec{\nabla}_\perp} \vec{\nabla}_\perp \phi(\tau') d\tau', \quad (29)$$

where the exponential denotes the corresponding Taylor series expansion (and ϕ on the RHS is again evaluated on the z -axis). We can find all terms linear in ϕ in the solution by substituting for $\vec{x}_\perp(\tau')$ in the RHS the ϕ -independent term $-(\tau_0 - \tau')\vec{n}_\perp^0$. We now find that

$$\begin{aligned} l_\perp^i(\tau) &= -\theta^i + 2 \int_\tau^{\tau_0} \left[e^{(\tau_0 - \tau')\vec{\theta} \cdot \vec{\nabla}_\perp} - 1 \right] \partial^i \phi(\tau') d\tau', \\ d_\perp^i(\tau) &= (\tau_0 - \tau)\theta^i - 2 \int_\tau^{\tau_0} (\tau' - \tau) \left[e^{(\tau_0 - \tau')\vec{\theta} \cdot \vec{\nabla}_\perp} - 1 \right] \partial^i \phi(\tau') d\tau'. \end{aligned} \quad (30)$$

If we let $\vec{p}_\perp = \vec{l}_\perp(\tau_L) + \vec{\gamma}(\vec{d}_\perp^L)$ then between the lens and the source we similarly find that

$$\begin{aligned} l_\perp^i(\tau) &= p_\perp^i + 2 \int_\tau^{\tau_L} \left[e^{(\vec{d}_\perp^L - (\tau_L - \tau')\vec{p}_\perp) \cdot \vec{\nabla}_\perp} - 1 \right] \partial^i \phi(\tau') d\tau', \\ d_\perp^i(\tau) &= d_\perp^i(\tau_L) - (\tau_L - \tau)p_\perp^i - 2 \int_\tau^{\tau_L} (\tau' - \tau) \left[e^{(\vec{d}_\perp^L - (\tau_L - \tau')\vec{p}_\perp) \cdot \vec{\nabla}_\perp} - 1 \right] \partial^i \phi(\tau') d\tau'. \end{aligned} \quad (31)$$

The lens equation is

$$\beta^i = \theta^i - \alpha^i - \frac{2}{r_S} \int_{\tau_L}^{\tau_0} (\tau - \tau_S) \left[e^{(\tau_0 - \tau)\vec{\theta} \cdot \vec{\nabla}_\perp} - 1 \right] \partial^i \phi(\tau) d\tau$$

$$-\frac{2}{r_S} \int_{\tau_S}^{\tau_L} (\tau - \tau_S) \left[e^{((\tau_0 - \tau)\vec{\theta} - (\tau_L - \tau)\vec{\gamma}) \cdot \vec{\nabla}_\perp} - 1 \right] \partial^i \phi(\tau) d\tau, \quad (32)$$

with $\vec{\alpha}$ and $\vec{\gamma}$ evaluated at \vec{d}_\perp^L calculated from equation (30). The magnification matrix is

$$\frac{\partial \beta^i}{\partial \theta_j} = \delta^{ij} + A^{ij} - \Psi^{ij} - B^{ij}, \quad (33)$$

where

$$\begin{aligned} A_{ij} &= -\frac{2}{r_S} \int_{\tau_L}^{\tau_0} e^{(\tau_0 - \tau)\vec{\theta} \cdot \vec{\nabla}_\perp} (\tau - \tau_S) (\tau_0 - \tau) \partial_i \partial_j \phi(\tau) d\tau \\ &\quad - \frac{2}{r_S} \int_{\tau_S}^{\tau_L} e^{((\tau_0 - \tau)\vec{\theta} - (\tau_L - \tau)\vec{\gamma}) \cdot \vec{\nabla}_\perp} (\tau - \tau_S) (\tau_0 - \tau) \partial_i \partial_j \phi(\tau) d\tau, \\ B_{ij} &= -\frac{2}{r_L} \Psi_i^k \int_{\tau_L}^{\tau_0} e^{(\tau_0 - \tau)\vec{\theta} \cdot \vec{\nabla}_\perp} (\tau - \tau_L) (\tau_0 - \tau) \partial_k \partial_j \phi(\tau) d\tau \\ &\quad - \frac{2}{r_{LS}} \Psi_j^k \int_{\tau_S}^{\tau_L} e^{((\tau_0 - \tau)\vec{\theta} - (\tau_L - \tau)\vec{\gamma}) \cdot \vec{\nabla}_\perp} (\tau - \tau_S) (\tau_L - \tau) \partial_k \partial_i \phi(\tau) d\tau. \end{aligned}$$

If we expand the exponentials to first order in equation (32) and zeroth order in equation (33), we recover the results of §3. If lensing is not strong, B_{ij} is small, and in the external shear A_{ij} we can set $\vec{\gamma} = (\vec{\theta} - \vec{\beta})r_S/r_{LS}$. In the limit of weak lensing, we can set $\vec{\gamma} = 0$ to get

$$A_{ij} = -\frac{2}{r_S} \int_{\tau_S}^{\tau_0} e^{(\tau_0 - \tau)\vec{\theta} \cdot \vec{\nabla}_\perp} (\tau - \tau_S) (\tau_0 - \tau) \partial_i \partial_j \phi(\tau) d\tau. \quad (34)$$

This expression can be used to calculate two point correlation functions of ellipticity. E.g., we can write down $\langle \text{Tr}A(\theta = 0) \text{Tr}A(\theta) \rangle$ and evaluate this expectation value in Fourier space. The exponential of $i r \vec{\theta} \cdot \vec{k}$ (in Fourier space) oscillates rapidly at high k , which cuts off small wavelengths and prevents any divergence. The result, which is derived fully in Appendix B, agrees with previous analyses of weak lensing in the absence of a primary lens (e.g. Blandford et al. 1991; Miralda-Escudé 1991; Kaiser 1992). These analyses have found that the relative change in the angular correlation of ellipticity is smaller than 10% (in an r.m.s. sense) for θ less than about an arcminute. For the non-linear spectrum, we find this to be true below about $10''$ (see also Seljak 1995), thus justifying our keeping only linear terms in $\vec{\theta}$ for strong lensing. Our result (33) is more general than weak lensing, as it includes a primary lens (Ψ^{ij}) and cross-terms (B^{ij}).

We can also get quadratic and higher-order terms in the gradients of ϕ by iterating this procedure. Given a solution $\vec{x}_\perp^{(j)}$ we substitute it in the RHS of equation (29) and find the next order solution $\vec{x}_\perp^{(j+1)}$. The exponential of $i \vec{k} \cdot \vec{x}_\perp^{(j)}$ ensures that small wavelength modes are cut off in the calculation of $\vec{x}_\perp^{(j+1)}$. This corresponds to the physical intuition that on average $\phi(r\hat{z} + \vec{x}_\perp^{(j)}) - \phi(r\hat{z})$ is determined by power on scales of order $|\vec{x}_\perp^{(j)}|$. If we calculate the r.m.s. shear at a point (i.e. for $\theta = \gamma = 0$) corresponding to $\vec{x}_\perp^{(j+1)}$, for a given $\vec{x}_\perp^{(j)}(\tau)$, the answer is the same as for $\vec{x}_\perp^{(j)}(\tau) = 0$ as long as the angular deflection is small and LSS power on the scale of r_S is negligible. There is, of course a statistical correlation between $\vec{x}_\perp^{(j)}(\tau)$ and $\phi(\tau)$, but it is typically weak since $\vec{x}_\perp^{(j)}(\tau)$ is determined by the accumulated deflection from

τ to τ_0 , a distance many times larger than the coherence length of LSS. The first correction to F_{OS} is a relative correction of order 1%, if ϕ is Gaussian, and the corrections to F_{OS} are expected to be small also for a non-Gaussian ϕ produced through hierarchical clustering.

8. Conclusions

We have shown that LSS can have significant effects on strong gravitational lensing. This suggests that lens reconstruction done without including LSS might reach incorrect conclusions about the distribution of matter in the lensing galaxy or cluster. It also raises the possibility of constraining the amplitude of the power spectrum directly, if lensing observations can be used to detect the effect of LSS.

The effect of LSS is simply described by two symmetric tensors. Including only the effect of F_{eff} , we find that the observed power spectrum of LSS requires the presence of an external shear of order 6% if $z_S = 3$. This can significantly affect the cross sections for image multiplicities in lens systems. In particular, it can produce more images than would be created in the absence of LSS. This implies that in addition to the usual magnification bias, which increases the observed number of quads relative to doubles, there is a bias in quads toward lines of sight with relatively large effective shear from LSS.

The second effect, given by F_{OL} , produces a magnification and shear between the observer and the lens. This term enters the lens equation differently from the effective shear and should be included in lens modelling. It also distorts the lens plane, which contributes an ellipticity to the observed lens galaxy, and converts the angular diameter “distance” into a tensor, though the comoving distance is still simply defined in terms of the observed redshift. Even if lens reconstruction can model the lens potential exactly, we find that LSS creates an absolute uncertainty ($\approx 5 - 10\%$ at 1σ) in deductions of the Hubble constant from time delays. Among lens systems, the uncertainty is smaller for those with lower lens and source redshifts.

Models of quadruple lenses typically find a shear of order 10% in addition to an axi-symmetric mass distribution. If this is due to the ellipticity of the lens galaxy, it may imply a larger ellipticity than that observed in the galaxy light distribution, as confirmed in a number of cases by recent observations. Since quads tend to be produced more easily when the shear due to the galaxy and the effective shear due to LSS are aligned, it is important to compare the magnitudes of the observed and modeled shears for consistency, and not only their directions. If the shear is due instead to other galaxies or clusters near the line of sight to the source, these additional lenses may not be found where expected. Only high-resolution observations and careful modelling of particular lens systems will determine if the shear may in part be due to LSS. When the parameters of many lenses are confidently known, it may become possible to study the redshift dependence of the shear. E.g., LSS does not affect lens reconstruction if the lens is at very low redshift. The original Einstein Cross 2237+0305 has $z_L = 0.04$, $z_S = 1.7$, and the lens light distribution seems to be consistent with the lensing mass (Rix et al. 1992). Other methods must be used to investigate independently whether the mass in galaxies is more flattened than the light distribution or not. E.g., an affirmative answer is suggested by an optical plus X-ray study of the elliptical galaxy NGC 720 (Buote & Canizares 1994).

Constraining the effects of LSS on strong lensing should complement observations of weak lensing due

to LSS. For measurements of weak lensing the sources are background galaxies, and the interpretation is complicated by the unknown source redshift distribution, while for some strong lenses the redshifts of the lens and source are known. If the characteristic source redshift for weak lensing is $\approx 0.7 - 1$ then the shear due to LSS is significantly smaller than for strong lensing (e.g. figure 2). In addition, since measurements of weak lensing with high signal to noise require relatively large angular fields, the r.m.s. shear is further reduced. On the other hand, weak lensing due to LSS can in principle be distinguished from other effects by averaging over a wide field, an option not available in strong lensing. Demanding consistency between determinations of the effects in these two regimes should allow us to learn more about the distribution of matter in the universe.

I thank Ed Bertschinger for suggesting this problem and for helpful advice, Uroš Seljak for valuable discussions and for his computer program to calculate r.m.s. shear, Paul Schechter for helpful discussions and comments, and the referee Josh Frieman for valuable comments. This work was supported by NASA grant NAG5-2816.

A. Appendix A

To calculate LSS shear in a curved background requires slight modifications of our formulas (e.g. Miralda-Escudé 1991; Seljak 1995). In a general Robertson-Walker model, the line element is

$$ds^2 = a^2(\tau) \left[-(1 + 2\phi)d\tau^2 + (1 - 2\phi)[d\chi^2 + \sin_K^2 \chi (d\theta^2 + \sin^2 \theta d\phi^2)] \right], \quad (\text{A1})$$

in terms of spherical comoving coordinates, where we are now using the variable $\chi = \tau_0 - \tau$. We have defined

$$\sin_K \chi \equiv \begin{cases} K^{-1/2} \sin K^{1/2} \chi & \text{if } K > 0. \\ \chi & \text{if } K = 0. \\ (-K)^{-1/2} \sinh(-K)^{1/2} \chi & \text{if } K < 0. \end{cases} \quad (\text{A2})$$

The curvature is $K = (\Omega_0 - 1)H_0^2$. The relation between redshift and τ is given by the Friedmann equation.

In a curved geometry, a deflection by angle $\delta\vec{\theta}$ at χ' leads to a perpendicular displacement at χ of $\delta\vec{x}_\perp = \delta\vec{\theta} \sin_K(\chi - \chi')$. In our approximation of §3, these deflections simply add linearly. Thus, our expressions for \vec{x}_\perp or \vec{d}_\perp remain valid if we replace any expression of the form $\tau_1 - \tau_2$ with $\sin_K(\tau_1 - \tau_2)$, so e.g. $r_{LS} = \sin_K(\tau_L - \tau_S)$. Thus the lens equation (14), the magnification matrix (16), and (again by Fermat's principle) the time delay (21) all have the same form except that now

$$F_{ij}(\tau_1, \tau_2) = -\frac{2}{\sin_K(\tau_1 - \tau_2)} \int_{\tau_2}^{\tau_1} \sin_K(\tau - \tau_2) \sin_K(\tau_1 - \tau) \partial_i \partial_j \phi(\tau) d\tau. \quad (\text{A3})$$

B. Appendix B

In the limit of weak lensing with no primary lens, our formalism reproduces previously derived results. From equation (34), we find

$$\langle \text{TrA}(\theta = 0) \text{TrA}(\theta) \rangle = \frac{4}{r_S^2} \int_0^{r_S} dr_1 \int_0^{r_S} dr_2 e^{r_1 \vec{\theta} \cdot \vec{\nabla}_\perp} r_1 (r_S - r_1) r_2 (r_S - r_2) \left\langle \vec{\nabla}_\perp^2 \phi(\tau_1) \vec{\nabla}_\perp^2 \phi(\tau_2) \right\rangle ,$$

where we have used $r_1 = \tau_0 - \tau_1$, etc. We convert to Fourier space, and use spherical coordinates $\{k, \theta_k, \phi_k\}$. We use the approximation that only k values for which $kr_S \gg 1$ (i.e., wavelengths much smaller than the source distance) make an important contribution. This implies that $\int_0^{r_S} dr_1 \int_0^{r_S} dr_2 \approx \int_0^{r_S} dr_1 \int_{-r_S}^{r_S} du$, with $u = r_2 - r_1$, and also that we can set $r_2 = r_1$ in the distance terms in the integrand. Letting $\omega = ku$ and denoting r_1 now by r , in Fourier space our expression becomes

$$4 \int_0^{r_S} dr \int_{-kr_S}^{kr_S} d\omega \int d^3k e^{ikr\theta \sin\theta_k \cos\phi_k} e^{i\omega \cos\theta_k} \sin^4\theta_k r^2 \left(1 - \frac{r}{r_S}\right)^2 k^3 P_\phi(k, \tau = \tau_0 - r) ,$$

where in the \vec{k} integration we chose the x -axis in the direction of $\vec{\theta}$. Under the approximation of $kr_S \gg 1$,

$$\int_{-kr_S}^{kr_S} d\omega e^{i\omega \cos\theta_k} = 2\pi \delta(\cos\theta_k) .$$

Our expression thus equals

$$8\pi \int_0^{r_S} dr r^2 \left(1 - \frac{r}{r_S}\right)^2 \int_0^\infty k^5 dk P_\phi(k, \tau = \tau_0 - r) \int_0^{2\pi} d\phi_k e^{ikr\theta \cos\phi_k} ,$$

or, finally,

$$\langle \text{TrA}(\theta = 0) \text{TrA}(\theta) \rangle = 16\pi^2 \int_0^{r_S} dr r^2 \left(1 - \frac{r}{r_S}\right)^2 \int_0^\infty k^5 dk P_\phi(k, \tau = \tau_0 - r) J_0(kr\theta) . \quad (\text{B1})$$

This correlation function of Tr A equals that of twice the shear of A , which has also been derived previously through other methods (e.g. Blandford et al. 1991; Miralda-Escudé 1991; Kaiser 1992).

REFERENCES

- Babul, A., & Lee, M. H. 1991, MNRAS, 250, 407
- Bardeen, J. M. 1980, Phys. Rev. D, 22, 1882
- Bardeen, J. M., Bond, J. R., Kaiser, N., & Szalay, A. S. 1986, ApJ, 304, 15
- Blandford, R. D., Saust, A. B., Brainerd, T. G., & Villumsen, J. V. 1991, MNRAS, 251, 600
- Buote, D. A., & Canizares, C. R. 1994, ApJ, 427, 86
- Cen, R., Gnedin, N. Y., Kofman, L. A., & Ostriker, J. P. 1992, ApJ, 399, L11

- Eisenhardt, P. R., Armus, L., Hogg, D. W., Soifer, B. T., & Neugebauer, G., to appear in ApJ 10 April 1996, preprint astro-ph/9510093
- Falco, E. E., Gorenstein, M.V., & Shapiro, I. I. 1985, ApJ, 289, L1
- Falco, E. E., Gorenstein, M.V., & Shapiro, I. I. 1991, ApJ, 372, 364
- Hamilton, A. J. S., Kumar, P., Lu, E., & Matthews, A. 1991, ApJ, 374, L1
- Jain, B., Mo, H. J., & White, S. D. M. 1995, MNRAS, 276, L25
- Jaroszynski, M., Park, C., Paczynski, B., & Gott, J. R. 1991, ApJ, 365, 22
- Kaiser, N. 1992, ApJ, 388, 272
- Kassiola, A., & Kovner, I. 1993, ApJ, 417, 450
- Kochanek, C. S. 1991a, ApJ, 373, 354
- Kochanek, C. S. 1991b, ApJ, 379, 517
- Kochanek, C. S. 1995, ApJ, 453, 545
- Kovner, I. 1987, ApJ, 316, 52
- Lehár, J., Hewitt, J. N., Roberts, D. H., & Burke, B. F. 1992, ApJ, 384, 453
- Miralda-Escudé, J. 1991, ApJ, 380, 1
- Mould, J., Blandford, R., Villumsen, J., Brainerd, T., Smail, I., Small, T., & Kells, W. 1994, MNRAS, 271, 31
- Narayan, R. 1991, ApJ, 378, L5
- Peacock, J. A., & Dodds, S. J. 1994, MNRAS, 267, 1020
- Ratnatunga, K. U., Ostrander, E. J., Griffiths, R. E. & Im, M. 1995, ApJ, 453, L5
- Refsdal, S. 1964, MNRAS, 128, 307
- Refsdal, S. 1966, MNRAS, 132, 101
- Rix, H. W., Schneider, D. P., Bahcall, J. N. 1992, AJ, 104, 959
- Ryden, B. S. 1992, ApJ, 396, 445
- Sackett, P. D., in IAU Symposium 173, “Gravitational Lensing,” Melbourne, July 1995, eds. C. Kochanek and J. Hewitt, preprint astro-ph/9508098
- Schechter, P. L., 1987, IAU Symposium 127, “Elliptical Galaxies,” 217

- Schneider, P., Ehlers, J., & Falco, E.E. 1992, *Gravitational Lenses* (New York: Springer)
- Seljak, U. 1994, *ApJ*, 436, 509
- Seljak, U. 1995, preprint astro-ph/9505109
- Surpi, G. C., Harari, D. D., & Frieman, J. A. 1995, preprint astro-ph/9502008
- Vanderriest, C., Schneider, J., Herpe, G., Chevretton, M., Moles, M., & Wlérick, G. 1989, *A&A*, 215, 1
- Villumsen, J. V. 1995, preprint astro-ph/9507007
- Wallington, S., & Narayan, R. 1993, *ApJ*, 403, 517